Chinese Chemical Letters 34 (2023) 107895

Contents lists available at ScienceDirect

Chinese Chemical Letters

journal homepage: www.elsevier.com/locate/cclet

Surface-enhanced Raman scattering technology based on TiO_2/Nb_2C coated microfluidic chip for monitoring glioma cells invasion in real time

Jie Zhao[a], Xiaoyan Liu[a], Yan Zhou[b], Tingting Zheng[a,*], Yang Tian[a,b,*]

[a] Shanghai Key Laboratory of Green Chemistry and Chemical Processes, Department of Chemistry, School of Chemistry and Molecular Engineering, East China Normal University, Shanghai 200241, China
[b] State Key Laboratory of Precision Spectroscopy, East China Normal University, Shanghai 200241, China

ARTICLE INFO

Article history:
Received 22 August 2022
Revised 2 October 2022
Accepted 7 October 2022
Available online 14 October 2022

Keywords:
Surface-enhanced Raman spectroscopy
Microfluidic chips
VEGF
Glioma cells
Integration of diagnosis and treatment

ABSTRACT

Glioma is a malignant primary brain tumor that is extremely harmful to human beings. Therefore, studying the invasiveness of glioma cells is of great significance for the diagnosis and treatment of glioma. In this work, TiO_2/Nb_2C was prepared as a SERS substrate and combined with microfluidic chip to construct an invasion model capable of monitoring glioma invasion in real time. Both experimental data and density function theory (DFT) calculations showed that the significant SERS-enhancing effect of TiO_2/Nb_2C on methylene blue (MB) originated from the chemical magnification (CM) mechanism when MB was used as the adsorbed molecule. Based on this, we achieved a highly sensitive and targeted detection of vascular endothelial growth factor (VEGF), a biomarker for glioma with a low detection limit of 3.7 pg/mL, then quantified the invasive process in real time by detecting VEGF. Meanwhile, the depletion of reactive oxygen species (ROS) by TiO_2/Nb_2C can inhibit the invasion of glioma cells. For the first time, the invasion model combines SERS technology with microfluidic technology, while monitoring the cell invasion process in real time, the invasion process can be quantified by detecting the VEGF secreted by glioma cells during the invasion process, realizing the integration of diagnosis and treatment, and establish a new model for the biomedical analysis, clinical diagnosis and treatment of glioma.

Glioblastoma is the most common and aggressive primary brain tumor in adults, with a really short median survival of only 15 months [1]. Invasive glioblastoma cells evade surgery and focal therapy and are a major obstacle to curative therapy. Recently, there has been increasing interest in how crosstalk among the tumor microenvironment may affect glioma progression. Currently, standard treatments fail to target infiltrating tumor cells, and no effective anti-invasive therapeutic strategies are available [2]. Among non-immunogenic cell types in the brain, endothelial cells typically contribute to glioblastoma (GBM) growth and invasion [3], and VEGF can be used as a biomarker to quantify the invasion process [4]. Currently, various methods including chemiluminescence, electrochemical analysis, enzyme-linked immunosorbent assay (ELISA) and fluorescence immunoassay (FIA) are used to monitor VEGF. However, these methods often require complex sample preparation and instruments, which are time-consuming and expensive. Therefore, it is very important to develop an alternative detection method to detect VEGF sensitively and specifically. Compared to the above techniques, SERS is an attractive tool for the detection of trace VEGF due to its molecular fingerprint specificity and potential single-molecule sensitivity [5].

TiO_2 is a typical semiconductor material, with excellent photocatalytic performance and biocompatibility. However, compared with noble metal substrates, the Raman enhancement ability of TiO_2 is weak. Therefore, it is particularly necessary to further improve the Raman enhancement effect of TiO_2 as a SERS substrate by structural optimization. Some recent literature has shown that non-nobel metal substrate SERS performance can be effectively improved by strategies such as building heterojunctions [6–8]. MXenes, the emerging two-dimensional (2D) materials with huge specific surface area, favorable biocompatibility and electrical conductivity, have garnered great attention [9]. With atomically thin structure and the insufficient coordination number of its surface atoms, MXenes are promising to exhibit excellent SERS performance [10]. In addition, the abundant excited electrons outside the nucleus of Nb^{5+} promote charge transfer between semiconductors

* Corresponding authors:
E-mail addresses: ttzheng@chem.ecnu.edu.cn (T. Zheng), ytian@chem.ecnu.edu.cn (Y. Tian).

https://doi.org/10.1016/j.cclet.2022.107895
1001-8417/

and molecules, as well as facilitate the generation of vacancy defects [11]. Combining the advantages, the composites of Nb_2C and TiO_2 may exhibit excellent SERS performance.

Microfluidics enables the construction of 3D structures with controlled spatial relationships, and allows precise control of the chemical environment in the system for replicating the chemical gradients at which microenvironmental structures are located *in vivo* [12–14]. The combination of SERS technology and microfluidics makes it possible to better simulate the physiological environment and obtain quantitative measurements [15,16].

In this study, we designed a microfluidic platform based on TiO_2/Nb_2C composites, to real-time monitor the invasion process of glioma, quantitatively analyze VEGF by SERS technology. When using MB molecule as the absorption molecule, both experimental data and DFT calculations showed that the significant SERS enhancement effect with enhanced factor (EF) value of 1.07×10^6 was derived from the CM mechanism. In the invasion model, we used the target-induced structure switching of the hairpin aptamer to develop an aptamer recognition-trigged SERS probe with MB and TiO_2/Nb_2C to achieve VEGF detection with high sensitivity and specificity, with a detection limit as low as 3.7 pg/mL. Reactive oxygen species in tumors have been suggested to induce a variety of physiological processes including invasion. Since MXene exhibited excellent antioxidant properties, the TiO_2/Nb_2C composites could reduce invasiveness of U87 MG cells by ROS scavenging. Using fluorescence and SERS technology, we observed and quantified the invasion process of glioma cells in real time, realized the integration of diagnosis and treatment and established a new model for the biomedical analysis, clinical diagnosis and treatment of glioma.

First, TiO_2 nanorod array structure was synthesized on fluorine doped tin oxide coated glass (FTO-glass) substrate with hydrothermal method [17]. To get the TiO_2/Nb_2C composites, Niobium carbide (Nb_2C) was obtained by etching Nb_2AlC with HF, and then spin-coated on the TiO_2 nanorod array and was calcined with a tube furnace. The synthesized TiO_2/Nb_2C composites were subjected to a series of characterizations to investigate its structure and composition. Scanning electron microscope (SEM) images in Fig. S1 (Supporting information) showed that TiO_2 exhibited a typical rod-like structure with an average diameter of about 200 nm, while the Nb_2C showed an accordion-like structure with interlayer spacing of 1.79 nm after exfoliation [18]. Few layers of Nb_2C uniformly covering the TiO_2 surface and formed the TiO_2/Nb_2C composite (Fig. 1a). As shown in Fig. 1b, the high-resolution transmission electron microscopy (HRTEM) image revealed a lattice fringe of 0.35 nm, corresponding to the (101) plane of TiO_2. Furthermore, the energy dispersive spectroscopy (EDS) mapping in Fig. 1c confirmed the presence of Nb, Ti and C elements in TiO_2/Nb_2C. The X-ray diffraction (XRD) pattern (Fig. 1d) showed the diffraction peaks at 25.3°, 37.8°, 62.7° and 70.3° indexed to the characteristic (101), (004), (204) and (220) plane, matched well with XRD pattern of anatase TiO_2. And the (002) peak of Nb_2C downshifted significantly toward a lower 2θ angle of 8.1° after exfoliation [19]. Meanwhile, X-ray photoelectron spectroscopy (XPS) was used to illustrate the chemical bonding in TiO_2/Nb_2C (Fig. 1e). The Nb 3d spectrum showed three peaks at 204.6, 207.6 and 210.1 eV designating to Nb-C bond, Nb $3d_{5/2}$ and $3d_{3/2}$ in Nb_2O_5, respectively. The C 1s spectrum exhibited three peaks at 281.5, 284.8 and 285.7 eV designating to C-Nb, C-C and C-O bond. The two peaks of Ti 2p at 458.8 and 464.6 eV corresponding to Ti $2p_{3/2}$ and $2p_{1/2}$ were also observed. From O 1s spectrum, three peaks at 530.1, 531.4 and 532.7 eV can be ascribed to three types of oxygen species, including the Ti-O bond, anionic oxygen in Nb_2O_5 and oxygen-containing functional groups of MXene [18,20]. All of these results revealed the TiO_2/Nb_2C composites were successfully synthesized.

In the UV-vis diffuse reflectance spectra (UV-vis DRS), the strong absorption of TiO_2/Nb_2C composites in the range of 200-400 nm was consistent with TiO_2, while the peak at 788 nm of high near-infrared (NIR) light absorption was assigned to Nb_2C (Fig. 1f) [21]. In the light of the photo-induced charge transfer (PICT) mechanism, the highest Raman enhancement can be obtained for the charge transfer (CT) complexes when the excitation frequency resonates with the electronic transitions. Therefore, 785 nm wavelength was chosen as the Raman excitation wavelength, which also reducing the damage to biological samples. Then, the SERS enhanced capability of TiO_2/Nb_2C was evaluated using methylene blue (MB) as a signal molecule. As shown in Fig. 1g, the Raman signal of MB was negligible on the bare Si substrates under 785 nm irradiation (black curve). However, a remarkable SERS effect was observed combined with TiO_2/Nb_2C (red curve), compared with both TiO_2 and Nb_2C substrates (green and blue curve). While 532 or 633 nm wavelength was used as the excitation laser wavelength (Fig. S3 in Supporting information), no significant enhancement was observed for the MB-TiO_2/Nb_2C probe, which reinforced that the MB-TiO_2/Nb_2C-CT complex undergone the most intensive PICT resonance when the excitation wavelength was 785 nm. The EF value of MB on the TiO_2/Nb_2C was calculated to be 1.07×10^6 (for details, see Supporting information). The PICT process was then further investigated by DFT calculations, which provided strong evidence for effective CT between TiO_2/Nb_2C and MB. As shown in Fig. 1h, the energy barrier between valence band (VB) and conduction band (CB) of Nb_2C was 1.5 eV. Thus, the photon energy of 785 nm laser (1.58 eV) could excite the electrons at VB of Nb_2C into the CB of Nb_2C, then transferred to the CB of TiO_2 at -4.2 eV and finally to the LUMO of the MB at -4.6 eV [22].

The TiO_2/Nb_2C with the superior SERS enhancement was then developed as a MB@TiO_2/Nb_2C probe to measure VEGF so as to monitor the process of glioma invasion. As illustrated in Scheme 1, VEGF hairpin aptamer labelled with MB molecule was attached to TiO_2/Nb_2C composites to form MB@TiO_2/NB_2C probe [23]. In the absence of MB, the immobilized aptamer chain remained unfolded, which hindered the charge transfer between the MB molecule and the TiO_2/Nb_2C composites. Yet in the presence of VEGF, the aptamer would fold into a target-specific stem-loop structure, which shortened the MB-substrate distance and enhanced electron transfer, leading to a significant enhancement of the Raman signal. Then, MB@TiO_2/Nb_2C was evaluated as a SERS probe for the *in vitro* detection of VEGF. The typical peak of MB at 1618 cm^{-1} indexed to C–C stretching ($\nu_{C\text{-}C}$) was selected as the characteristic peak. As shown in Fig. 2a, the intensity of the Raman peak at 1618 cm^{-1} (I_{1618}) gradually enhanced with increasing VEGF level. Meanwhile, the peak of 613 cm^{-1} attributed to the TiO_2 remained unchanged. Thus, to improve the accuracy, this peak was employed as an inner-reference [24]. The SERS intensity ratio (I_{1618}/I_{613}) showed a good linearity from 10 pg/mL to 1×10^4 pg/mL with LOD of 3.7 pg/mL (S/N = 3, n = 20, S.D.). The LOD was 10 times lower than those obtained by previous reported sensors (Fig. 2b, and Table S2 in Supporting information). Further, no obvious responses (<8.9%) were observed for other potential interferences (Fig. 2c), suggesting that this SERS platform possessed outstanding selectivity ascribe to the affinity of the aptamer to VEGF as well as the specific SERS enhancement effect of MB on TiO_2/Nb_2C.

In addition, the MXene with unique ROS scavenging ability is promising to be an outstanding candidate for the treatment of tumor [25–27]. At first, the antioxidant capacity of the TiO_2/Nb_2C composites was assessed by ultraviolet (UV) protection reaction, which inducing ROS generation such as $^{\bullet}OH$ and H_2O_2. The perceptibly color fading and lower corresponding absorbance of oxTMB in the reaction system with TiO_2/Nb_2C composites proved the ROS scavenging activity of the substrate (Fig. S5 in Supporting information). Besides, the substrate was tested by a salicylic

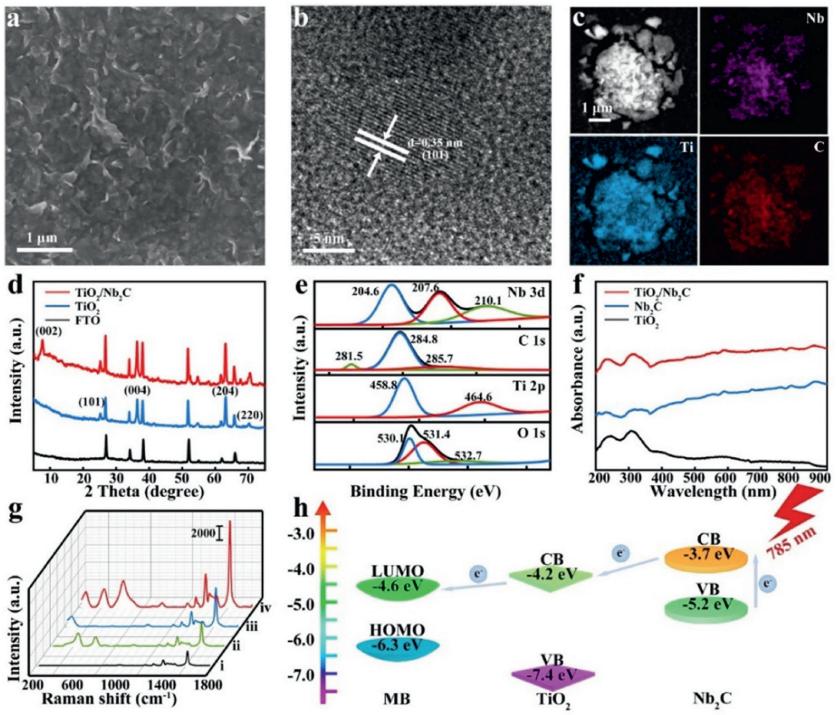

Fig. 1. (a) SEM image of TiO_2/Nb_2C-FTO. (b) HRTEM image of TiO_2/Nb_2C composites. (c) EDS mapping of TiO_2/Nb_2C composites. (d) XRD patterns of FTO-glass (black line), TiO_2-FTO (blue line) and TiO_2/Nb_2C-FTO (red line). (e) XPS survey spectrum of TiO_2/Nb_2C composites. (f) UV-vis spectra of TiO_2 (black line), Nb_2C (blue line) and TiO_2/Nb_2C (red line). (g) Raman spectra of the MB on TiO_2/Nb_2C-FTO (red line), MB on Nb_2C (blue line), MB on TiO_2 (green line) and MB on Si (black line). (h) Conclusion of the mechanism in the TiO_2/Nb_2C-MB system.

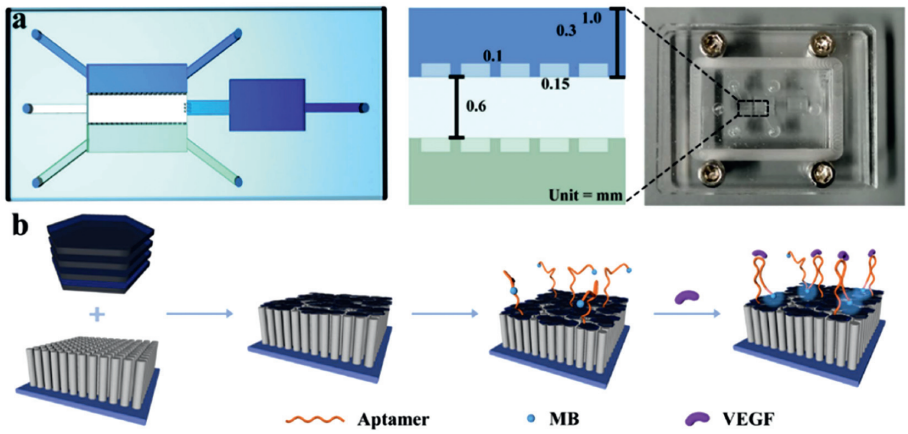

Scheme 1. (a) Structure of multifunctional microfluidic chip. (b) Schematic illustration of the sensing mechanism of MB@TiO_2/Nb_2C.

acid (SA) probe to evaluate the •OH scavenging ability [28]. After adding the TiO_2/Nb_2C composites, the •OH scavenging ratio showed concentration-dependent characteristics, where a higher concentration of TiO_2/Nb_2C composites resulted in stronger scavenging efficacy (Fig. S6 in Supporting information). There has been report demonstrated that the formation of intracellular ROS can be induced by the extracellular ROS [19]. Thus, confocal laser scanning microscopy (CLSM) analysis validated the intracellular radicals scavenging effect of TiO_2/NB_2C composites using 2′,7′-dichlorofluorescin diacetate (DCFH-DA). Although t he addition of Fe(II)/H_2O_2 could produce ROS and resulted in the progressive increments in DCF fluorescence, Nb_2C exposed U87 MG cells hardly showed fluorescence, suggesting the outstanding ROS scavenging activity of MXene [26]. In addition, TiO_2-exposed cells showed slightly enhanced fluorescence, which may be due to the photocatalytic capacity of TiO_2. Moreover, as for the cells applied to TiO_2/Nb_2C probe, much weaker fluorescence was observed compared with the control group, indicating a good ROS scavenging potential of the substrate (Fig. 2d). Then, methyl thiazolyl tetrazolium (MTT) was used to evaluate the cytocompatibility (Fig. S7 in Supporting information) When the concentration of TiO_2/Nb_2C composites reached 5 mg/mL, the probe still showed no acute toxicity to endothelial cells and glioma cells, demonstrating the potential for in situ biological applications.

Then, a microfluidic platform based on MB@TiO_2/Nb_2C was designed as an invasion model to monitor and quantify glioma invasion progress in real time [29,30]. The microfluidic SERS chip was developed with two main chambers for cells invasion observation and VEGF detection, respectively. As shown in Scheme 1a, the cell culture chamber was divided into three parallel channels by two rows of PDMS cuboid structure. The outer channel was used to culture U87 MG cells and endothelial cells, respectively,

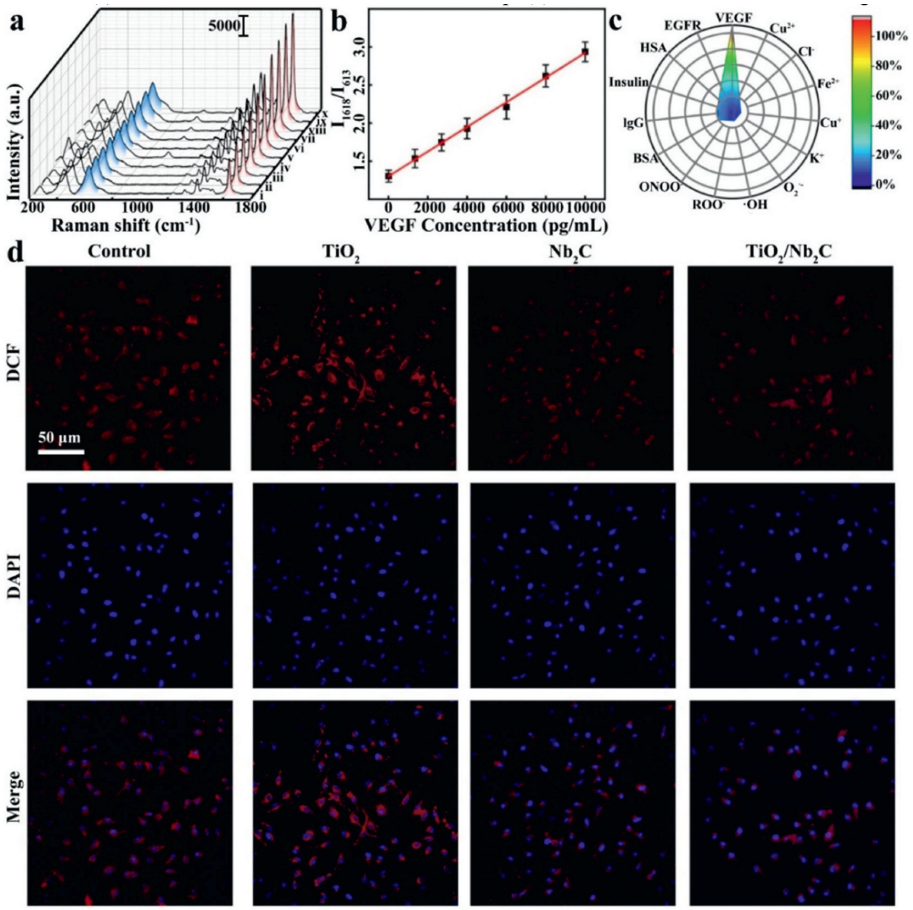

Fig. 2. (a) SERS spectra of VEGF with MB@TiO_2/Nb_2C (i-x: 10, 1350, 2700, 4000, 6000, 8000, 10000, 20000, 35000 and 50000 pg/mL). (b) SERS intensity ratio I_{1618}/I_{613} *versus* VEGF concentration. (c) Selectivity tests of SERS for VEGF monitoring against other potential interferences. (d) CLSM images of differently treated U87 MG cells stained with DCFH-DA.

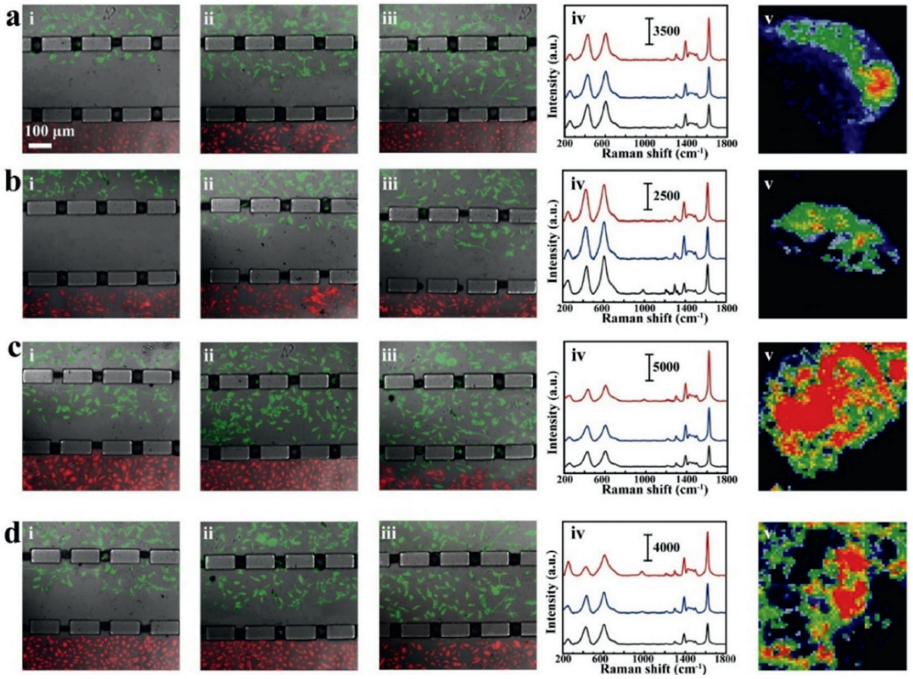

Fig. 3. Invasion of U87 MG cells induced by (a) control, (b) TiO_2/Nb_2C, (c) TGF-β, and (d) TiO_2/Nb_2C and TGF-β during 7 days. (i-iii) CLSM images in cell culture chamber incubated for 0, 4, 7 days. U87 MG cells and endothelial cells were stained by Calcein AM (green) and DiO (red), respectively. (iv) SERS spectra in SERS detection chamber incubated for 0 (black), 4 (blue), and 7 (red) days. (v) SERS images in SERS detection chamber incubated for 7 days.

and the middle channel was filled with Matrigel [31]. This design successfully enabled direct observation of the invasion process of U87 MG cells. At the same time, in the SERS detection chamber, the MB@TiO_2/Nb_2C probe on the FTO-glass realized VEGF continuous capture and on-line SERS analysis.

Previous studies had indicated that the upregulation of ROS will promote cell metastasis, thereby increasing cell invasiveness [32,33]. Therefore, we supposed that the TiO_2/Nb_2C substrate can inhibit U87 MG cells invasion by scavenging ROS in the microenvironment. Here, transforming growth factor beta (TGF-β) was used to induce tumor cell migration and invasion [34,35]. As shown in Fig. 3a, i-iii, during the 7 days of incubation, U87 MG cells would migrate to the endothelial cells, and the VEGF corresponding peak intensity at 1618 cm^{-1} increased (Fig. 3a, iv). The Raman intensity ratio (I_{1618}/I_{613}) also increased from 0.88 $\pm$ 0.06 to 1.75 $\pm$ 0.10 (black line in Fig. S8 in Supporting information). However, when only TiO_2/Nb_2C composites were added (group b), the invasion rate of U87 MG slowed down (Fig. 3b, i-iii), and I_{1618}/I_{613} increased more slowly, which reached 1.26 $\pm$ 0.09 on day 7 (red line in Fig. S8 in Supporting information). As for the group with only TGF-β (group c), the invasion rate of U87 MG was significantly accelerated (Fig. 3c, i-iii), and the intensity of I_{1618} also increased, up about 68% compared with control group (Fig. 3c, iv). Moreover, I_{1618}/I_{613} increased more rapidly and reached 2.94 $\pm$ 0.16 on the 7^{th} day (blue line in Fig. S8 in Supporting information). After the addition of TiO_2/Nb_2C composites and TGF-β (group d), the invasion effect was weakened compared with that in the presence of TGF-β alone. Correspondingly, the intensity of I_{1618} decreased by 25% compared with group c (Fig. 3d), and the final I_{1618}/I_{613} reached 2.21 $\pm$ 0.11 on day 7. The results of Raman mapping further confirmed the effect of different additives on VEGF concentration, which demonstrated that the TiO_2/Nb_2C composites can inhibit the invasion of U87 MG cells by depleting ROS (Figs. 3a-d, v). Collectively, the microfluidic SERS platform that we designed can observe glioma cell invasion and quantify this process as well.

In conclusion, we constructed a microfluidic SERS platform with TiO_2/Nb_2C complex as SERS substrate, which can be used as a glioma invasion model to achieve direct observation and quantification of the glioma invasion process. When MB molecule was used as the adsorption molecule, TiO_2/Nb_2C showed a significant enhancement of the Raman signal with an EF value of 1.07×10^6. Through experimental data and theoretical calculations, we found that this phenomenon originated from the CM mechanism, and the multiple transfers of excited electrons under 785 nm excitation resulted in the great enhancement of the Raman signal. Subsequently, SERS probe for VEGF monitoring was fabricated, combining the target-induced structure switching hairpin aptamer. After binding to the glioma biomarker VEGF, MB tagged on the aptamer moved closer to the surface of the substrate and the charge transfer enhanced the Raman signal, achieving a highly sensitive, specific detection of VEGF with a LOD as low as 3.7 pg/mL. Furthermore, the microfluidic technology allowed the integration of cell co-culture with biosensor to monitor the glioma cell invasion process in real time as well as to quantify the invasion process by detecting VEGF secreted by glioma cells during invasion. Additionally, the invasion ability of glioma cells was inhibited by TiO_2/Nb_2C for its ROS-scavenging ability, which offered the possibility of glioma diagnosis and treatment simultaneously. Therefore, we envision this approach as a potential tool in the biomedical analysis and clinical treatment of gliomas.

Declaration of competing interest

The authors declare that they have no known competing financial interests or personal relationships that could have appeared to influence the work reported in this pape

Acknowledgments

The authors are greatly grateful for the financial support from the National Natural Science Foundation of China (No. 21827814 for Y. Tian, No. 21974049 for T. Zheng). Besides, this work was also funded by Shanghai Rising-star Program (No. 20QA1403300) and Innovation Program of Shanghai Municipal Education Commission (No. 201701070005E00020).

Supplementary materials

Supplementary material associated with this article can be found, in the online version, at doi:10.1016/j.cclet.2022.107895.

References

[1] F.A. Desland, A. Hormigo, Int. J. Mol. Sci. 21 (2020) 7358.
[2] Q. Xie, S. Mittal, M.E. Berens, Neuro-Oncol. 16 (2014) 1575–1584.
[3] X.F. Gao, Z.H. Zhang, T. Mashimo, et al., Cell Rep. 30 (2020) 2489–2500 e5.
[4] Q.G. D'Alessandris, M. Martini, T. Cenci, et al., Neurology 84 (2015) 1906–1908.
[5] Y. Xue, D. Liu, X. Wang, et al., Chin. Chem. Lett. 33 (2022) 1595–1598.
[6] Y. Zhou, Q.Y. Gu, T.Z. Qiu, et al., Angew. Chem. Int. Ed. 60 (2021) 26260–26267.
[7] X.X. Han, W. Ji, B. Zhao, Y. Ozaki, Nanoscale 9 (2017) 4847–4861.
[8] P. Xue, S. Ye, H. Su, S. Wang, et al., Nanoscale 9 (2017) 6724–6733.
[9] X.Y. Ren, M.F. Huo, M.M. Wang, et al., ACS Nano 13 (2019) 6438–6454.
[10] M. Naguib, V.N. Mochalin, M.W. Barsoum, Y. Gogotsi, Adv. Mater. 26 (2014) 992–1005.
[11] A. Sarycheva, T. Makaryan, K. Maleski, et al., J. Phys. Chem. C 121 (2017) 19983–19988.
[12] R. Ning, J. Fan, L. Kong, et al., Chin. Chem. Lett. 33 (2022) 2243–2252.
[13] S. Wang, R. Zhou, Y. Hou, M. Wang, X. Hou, Chin. Chem. Lett. 33 (2022) 3650–3656.
[14] S. Wang, X. Yang, F. Wu, et al., Small 16 (2020) 1905318.
[15] R. Panneerselvam, H. Sadat, E.M. Hohn, et al., Lab Chip 22 (2022) 665–682.
[16] J.J.S. Rickard, V. Di-Pietro, D.J. Smith, et al., Nature Biomed. Eng. 4 (2020) 610–623.
[17] B. Liu, E.S. Aydil, J. Am. Chem. Soc. 131 (2009) 3985–3990.
[18] Y.F. Yan, H. Han, Y.J. Dai, et al., ACS Appl. Nano Mater. 4 (2021) 11763–11769.
[19] M.A. Koo, B.J. Kim, H.L. Mi, B.J. Kwon, J.C. Park, ACS Appl. Mater. Interfaces 8 (2016) 28448–28457.
[20] W.G. Gao, X.M. Li, S.J. Luo, et al., J. Colloid Interface Sci. 585 (2021) 20–29.
[21] L. Gao, C. Ma, S. Wei, A.V. Kuklin, H. Gren, ACS Nano 15 (2021) 954–965.
[22] Q. Xu, J. Ma, W. Khan, et al., Chem. Commun. 56 (2020) 6648–6651.
[23] S. González, Molecules 26 (2021) 3780–3795.
[24] S. Dehghani, R. Nosrati, M. Yousefi, et al., Biosens. Bioelectron. 110 (2018) 23–37.
[25] M. Gong, J. Xin, J. Du, et al., RSC Adv. 5 (2015) 80269–80275.
[26] W. Feng, X.G. Han, H. Hu, et al., Nature Commun. 12 (2021) 2203–2219.
[27] Y. Li, R.Z. Fu, Z.G. Duan, C.H. Zhu, D.D. Fan, ACS Nano 16 (2022) 7486–7502.
[28] H. Lin, S. Gao, C. Dai, Y. Chen, J. Shi, J. Am. Chem. Soc. 142 (2020) 10567-10567.
[29] X. Ren, M. Huo, M. Wang, H. Lin, H. Chen, ACS Nano 13 (2019) 6438–6454.
[30] G. Adriani, D. Ma, A. Pavesi, R.D. Kamm, E. Goh, Lab Chip 17 (2017) 448–459.
[31] T. Liu, B. Lin, J. Qin, Lab Chip 10 (2010) 1671–1677.
[32] W. Zhang, Z. He, L. Yi, et al., Biosens. Bioelectron. 102 (2018) 652–660.
[33] C.H. Hsieh, H.T. Chang, W.C. Shen, W.C. Shyu, R.S. Liu, Mol. Imag. Biol. 14 (2012) 489–499.
[34] H.L. Moses, Cytokine Growth Factor Rev. 21 (2010) 49–59.
[35] P.S. Smith, W. Zhao, M. Robbins, Cancer Res. 66 (2006) 1037-1037.